2021

Effects of shot peening on microstructure evolution and mechanical properties of surface nanocrystal layer on titanium matrix composite

Yan Wen

Yaya Wu

Lin Hua

Lechun Xie

Liqiang Wang

See next page for additional authors

10.1016/j.matdes.2021.109760

Wen, Y., Wu, Y., Hua, L., Xie, L., Wang, L., Zhang, L. C., & Lu, W. (2021). Effects of shot peening on microstructure evolution and mechanical properties of surface nanocrystal layer on titanium matrix composite. *Materials & Design, 206,* article 109760. https://doi.org/10.1016/j.matdes.2021.109760

Materials & Design 206 (2021) 109760

Contents lists available at ScienceDirect

Materials & Design

journal homepage: www.elsevier.com/locate/matdes

Effects of shot peening on microstructure evolution and mechanical properties of surface nanocrystal layer on titanium matrix composite

Yan Wen [a,b], Yaya Wu [a,b], Lin Hua [a,b,*], Lechun Xie [a,b,*], Liqiang Wang [c], Lai-Chang Zhang [d], Weijie Lu [c]

[a] Hubei Key Laboratory of Advanced Technology for Automotive Components, Wuhan University of Technology, Wuhan 430070, PR China
[b] Hubei Collaborative Innovation Center for Automotive Components Technology, Wuhan University of Technology, Wuhan 430070, PR China
[c] State Key Laboratory of Metal Matrix Composites, School of Materials Science and Engineering, Shanghai Jiao Tong University, No. 800 Dongchuan Road, Shanghai 200240, PR China
[d] School of Engineering, Edith Cowan University, 270 Joondalup Drive, Joondalup, Perth, WA 6027, Australia

HIGHLIGHTS

- The nanocrystal layers were introduced on the surface of Ti-6Al-4V and TMC by SP.
- The nanograin layers were influenced by the shape and distribution of reinforcements.
- Smaller nanograins near interfaces were formed via the severe deformation of matrix.
- The deformation of TiC was more severe than TiB because of the different shapes.
- The improved CRS and hardness on surface were due to the nanocrystal layer by SP.

GRAPHICAL ABSTRACT

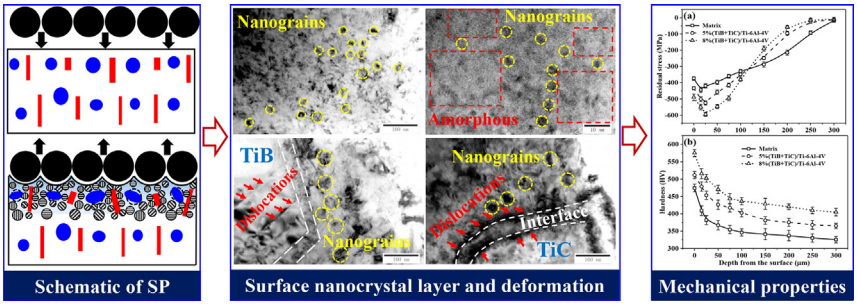

ARTICLE INFO

Article history:
Received 30 November 2020
Revised 14 April 2021
Accepted 20 April 2021
Available online 27 April 2021

Keywords:
Titanium matrix composite (TMC)
Shot peening (SP)
Transmission electron microscopy (TEM)
Nanograins
Reinforcements
Compressive residual stress (CRS)

ABSTRACT

Shot peening (SP) was employed to modify the surface microstructure and mechanical properties of (TiB+TiC)/Ti-6Al-4V titanium matrix composite (TMC). And the microstructure evolution and mechanical properties were characterized and analyzed in detail. Transmission electron microscopy (TEM) results illustrated that the surface nanograins were introduced by the effect of SP and the hindering of reinforcements to the matrix deformation. The nanograins were formed near the reinforcement/matrix interface because the matrix was squeezed by both the shots and the reinforcements. Moreover, with increasing the volume fraction of reinforcements, the smaller nanograins were introduced near the interfaces due to the severe deformation between the matrix and reinforcements, which were caused by the decrease in average distance between two reinforcements. Under the same intensity of SP, the deformation of TiC was more severe than that of TiB, and more dislocations were introduced around TiC. The results were influenced by both the different shapes and distribution of reinforcements, and the impact direction of shots. After SP, the compressive residual stress (CRS) and the hardness in the peened surface layer were improved, which was due to the surface deformation, nanograins and high dislocation density in the nanocrystal layer.

* Corresponding authors at: Hubei Key Laboratory of Advanced Technology for Automotive Components, Wuhan University of Technology, Wuhan 430070, PR China; Hubei Collaborative Innovation Center for Automotive Components Technology, Wuhan University of Technology, Wuhan 430070, PR China.
E-mail addresses: hualin@whut.edu.cn (L. Hua), xielechun@whut.edu.cn (L. Xie).

https://doi.org/10.1016/j.matdes.2021.109760
0264-1275/

1. Introduction

Titanium matrix composites (TMCs) have broad application prospects in the high-technology fields due to the larger modulus, the higher specific strength and the excellent performance at high temperature compared to titanium alloys [1–9]. TMCs have been manufactured to some important engine parts [10]. However, because of the different morphology of reinforcements, and the different physical and mechanical properties between reinforcements and matrix, the structural and thermodynamic mismatches between reinforcements and matrix are formed in the particle reinforced TMCs, which is apt to form the interface defects and stress concentration. The interface defects and stress concentration are easy to induce crack initiation and accelerate crack propagation, thereby limiting the fatigue properties of TMCs [11,12]. Therefore, it is great significance to manipulate the microstructure and mechanical properties to improve the fatigue performance of TMCs.

With respect to titanium alloys, some surface mechanical treatments were adopted to inhibit the initiation and growth of cracks on surface [13–15], such as the laser shocking peening (LSP) [16], the friction stir processing (FSP) [17,18] and the surface coatings [19]. The surface treatments of LSP and FSP would result in the large deformation and the phase transition in the surface layer, which are not appropriate for the treatment on TMCs because of the existence of reinforcements. The large deformation could cause the cracking and fracture of reinforcements, which would deteriorate the fatigue properties of TMCs. About the methods of surface coatings, it is difficult to guarantee the stability of interface between coatings and TMCs, especially the interfaces between coatings and reinforcemnets, since three or four phases exist in TMCs. Consequently, other surface treatment methods should be considered and adopted according to the special microstructure of TMCs.

As one of the most important and useful surface treatments, shot peening (SP) is widely utilized in industry [20–28] to improve surface properties of metallic components by inducing work hardening and compressive residual stress (CRS). During SP, a large number of high-hardness shots impact the surface of material, forming a plastic and elastic deformation layer on the surface. At the same time, the CRS and microstrain are introduced in the surface layer, and the surface grains are refined [29–32]. The effect of SP on Ti alloys have been done by many researchers. SP can modify the surface microstructure of Ti alloys. The CRS was introduced to a depth of 208 μm in the surface of shot peened Ti-6Al-4 V, and the maximum CRS increased from −130.6 MPa to −887 MPa, and the severe plastic deformation led to the large α-Ti grains and β-Ti strips to be refined into small grains with size of less than 1 μm [33]. The surface gradient nanocrystalline structure was obtained on TA17 alloy (Ti-4Al-2V) after SP, the grains were refined from 22 to 26 nm when shot peened at 0.6 MPa for 5 to 10 min, and the thickness of plastic deformation layer increased from 55 to 88 μm [34]. Nanostructure of 17 to 25 nm was developed in surface region of ultrasonic shot peened Ti-6Al-4V, up to the depth of 30 μm, and the nanostructured surface reduced the corrosion rate [35]. The laser peening and conventional SP deeply influenced the residual stress of selective laser melting (SLM) Ti-6Al-4V, whereas the laser peening showed much deeper stresses (up to 2.3 mm) compared to conventional SP (~ 443 μm) [36]. The influence of severe double SP on the microstructure of Ti-6Al-4V and titanium dissimilar joints were investigated, and the depths of peening pre-weldment and post peening weldment weldments were 8 μm and 10 μm respectively [37]. The composite layer including TA15 (Ti-6.5Al-2Zr-1.5Mo-1.5 V) and TC17 (Ti-5Al-4Mo-4Cr-2Zr-2Sn) was treated by the LSP, a high-level CRS (−596 MPa) and microstructure refinement were induced, and the average area of α phase decreased from 1.88 μm^2 to 0.73 μm^2, and much lower angle grain boundaries were generated [38]. Applying the rotationally accelerated SP on Ti-10V-2Fe-3Al alloys, the novel deformation twinning systems of $\{1\ 1\ 2\}_{\alpha''}$ and $\{1\ 3\ 0\}\ \langle 3\ 1\ 0\rangle_{\alpha''}$ in the kinked α″ martensite were revealed, and the stress-induced martensitic transformation, twinned α″ martensite and the grain refinement contributed to hardness and work hardening ability [39].

Meanwhile, SP can improve the mechanical properties of Ti alloys with the modification of surface microstructure. SP could effectively improve the fatigue performance of Ti-6Al-4V, the short crack propagation rate of SP specimen decreased by 34%–60%, the occurrence time of visible crack was delayed by 64.3%, and the fatigue life was increased by 34.2% [40]. An *in-situ* SP was introduced into cold spray to prepare dense Ti-6Al-4V coatings, the porosities of coatings were declined and the Vickers hardness of coatings increased from 240 HV to 427 HV [41]. The ultrasonic SP could effectively improve the corrosion resistance of the SLM Ti-6Al-4V [42]. The yield strength and the ultimate tensile strength of TC17 alloy processed by high energy SP were increased by 10.1% and 13.9%, respectively [43]. The TC17 blades were processed by milling-polishing (MP) and milling-polishing-SP-vibration polishing (MPSV), and the fatigue lives of the MPSV-processed blades were increased by approximately 119.5% compared with the MP-processed blades [44]. Usually, the severe SP or high energy SP could affect the microstructure obviously and introduce the surface nanocrystal layer, which are different to the conventional SP [45,46], so the concept of SP in this work means the high energy SP and the discussion will focus on the high energy SP. Due to the CRS and the refined grains, SP can greatly improve the fatigue strength, stress corrosion resistance and surface hardness [47,48]. Therefore, the advantages of SP can be adopted and utilized on TMCs to modify the surface properties.

SP has not been widely used in TMCs, some researches have been carried out on the distribution of residual stress in shot peened TMCs by means of X-ray diffraction (XRD) [31,32,49]. The CRS were induced on the surface layer, and the influence of reinforcements on CRS was obvious [32]. The effect of stress peening on surface characteristics was studied and it showed that the external loading on specimen before SP could improve the CRS and the thickness of deformation layer [31]. Besides, the results of numerical analysis showed that the CRS were introduced in the matrix, but the tensile residual stress generated in the reinforcements [49]. The surface microstructure of (TiC + TiB)/Ti-6Al-4V after SP was studied and analyzed by XRD, and the effects of SP intensities and reinforcements on the microstructure of surface were discussed [50–53]. Above investigations indicate that the influences of SP on CRS and surface microstructure are mainly manifested on the refinement of grains, the microstrain and the improvement of dislocation density. Note that, the surface deformation layer of shot peened TMCs were mainly characterized via utilizing XRD indirectly. There is little direct observation and characterization on the microstructure of deformation layer by electron microscopy.

As such, in this work, the surface microstructure of (TiB + TiC)/Ti–6Al–4V after SP, especially the nanograins, dislocation, lattice distortion, and so on, was characterized and analyzed by transmission electron microscopy (TEM), and the related mechanisms and mechanical properties were discussed, which are expected to provide the theoretical and experimental support for optimizing the SP parameters on TMCs.

2. Experimental procedure

2.1. Material preparation and SP treatment

(TiB + TiC)/Ti-6Al-4V (TiB:TiC = 1:1 (vol%)) were prepared by the in-situ method [54]. The microstructure and the lattice parameters could be found in our previous work [54–56]. The crystal structures of TiB is the orthorhombic structure with the lattice parameters of a = 0.612 nm, b = 0.306 nm, and c = 0.456 nm. The crystal structures of TiC is cubic structure with the lattice parameters of a = 0.435 nm. The volume fraction of raw material and the reinforcements in TMCs are shown in Table 1. The reinforcements of TiB and TiC were obtained by the following high-temperature chemical reactions: 5Ti + B_4C = 4TiB + TiC, Ti + C = TiC. Two kinds of TMCs with 5 vol% and 8 vol% reinforcements were obtained (Table 1). The TMCs bar with diameter of 15 mm were obtained by extrusion. The specimens used for SP were cut from the bar by wire-electrode cutting with the thickness of 3 mm and the diameter of 15 mm (Fig. 1). The SP process was carried out on the numerically controlled SP equipment, and the SP intensity was determined by using the arc height (mmA) of the standard Almen strip (type A). The SP intensity in this work was 0.15 mmA. The Al_2O_3 ceramic shots with the average diameter of 0.30 mm were utilized as the shot materials, and the average hardness of ceramic shots was about 700 HV. The nozzle diameter was 8 mm, and the distance between the nozzle and specimen was 100 mm. The coverage rate of SP was 200% in each step according to the calculation method in our previous work [49].

2.2. Microstructure characterization and mechanical properties evaluation

The schematic of the distribution of reinforcements along the radial and axial directions is shown in Fig. 1. The microstructure of corss-section has been shown and discussed in our previous work (shown in Fig. s1 in Support Information) [57]. Two kinds of reinforcements with different shapes were distributed uniformly in the matrix, along the radial direction, the TiB whiskers were short fibre-shaped, while the TiC particles were equiaxed or near equiaxed (Fig. 1(a)) [55,56]. But along the axial direction, the TiB whiskers were arranged along the axial direction because of the effect of hot forging during preforming (in Fig. 1(a)), and there was no significant of the distribution of TiC [55,56]; these results could be found in above references. Microstructure of the deformed surface layer after SP were characterized by TEM and high resolution TEM (HRTEM), using a JEM 2100 microscope operated at 200 kV equipped with energy dispersive spectrometer (EDS). The schematic of the deformation layer and the TEM observation area are shown in Fig. 1(b). In consideration of the surface roughness, the deformation layer with the thickness of 50 μm in subsurface were chosen to prepare the TEM specimens (Fig. 1 (b)), which were twin-jet polished in a solution with 3 vol. % perchloric acid and 97 vol% alcohol at −25 °C.

The XRD patterns of all samples were obtained by Rigaku Ultima IV X-ray diffractometer, which was operated at 40 kV/40 mA with Cu Kα radiation (λ = 1.54056 Å). The system

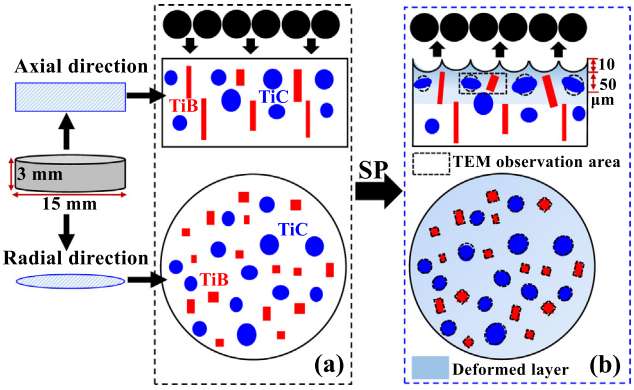

Fig. 1. Schematic of the specimen, the distribution of reinforcements along the radial and axial directions, the surface deformation layer and the TEM observation area after SP, (a) before SP; (b) after SP.

was set up with Bragg–Brentano optics for this study. The velocity of scan was 3°/min and the step of scan was 0.01°. The residual stress on the deformed layer were characterized by X-ray stress analyzer (LXRD, Proto, Canada), using Cu-*Ka* radiation and Ni filter under 30 kV and 25 mA. The residual stress were calculated by using the $\sin^2\psi$ method [58], the diffraction peak *(hkl)* of Ti (2 1 3) was chosen during measuring and the range of tilting angles was 0° – 45°. The α phase (*hcp*) was used for the residual stress measurement. The diffraction angle of 2θ = 139.69° and the stress constant of K = -262.86 MPa were determined for the X-ray stress measurement based on the formula of $K = -\frac{E}{2(1+\nu)}\cot\theta_0\frac{\pi}{180}$, and the constants of E = 110 GPa, ν = 0.34 and θ = 69.85°. The hardness was measured by Vickers Hardness Tester (DHV-1000, China) using an experimental load of 2.94 N, and five tests were performed and the average values were calculated. For obtaining the residual stress and hardness distributed along the depth, the surface layers were removed layer by layer via chemical etching, and the Kroll's solution (V_{HF} : V_{HNO3} : V_{H2O} = 7 : 12 : 31 in vol.%) was utilized for etching. Since the chemical corrosion rate was mainly related to the corrosion time and the concentration of solution [50], the chemical corrosion rates of Ti-6Al-4V and TMCs were about 7–10 μm/min.

3. Results

3.1. Surface nanocrystal layer in Ti-6Al-4 V and TMCs

The surface XRD patterns of Ti-6Al-4V and TMCs before and after SP are shown in Fig. 2. The XRD measurment was utilized to analyse the phases of α and β, and to characterize the full width at half maximum (FWHM) of some peaks, which can indicate the refinement of surface grains indirectly. Moreover, the XRD pattern was also utilized to check whether the phase transition exist, or some broken shots remained on the surface. According to this XRD, the diffraction peaks of Ti and reinforcements are shown and indexed, and there is no other phase generated or remained on the surface after SP. Moreover, the diffraction peaks of peened specimen become wider due to the refined domain size. In TMCs,

Table 1
The raw material composition and the reinforcements in TMCs.

Materials	Raw materials (wt.%)					Reinforcements (vol.%)
	AlV	Al	B_4C	C	Ti	TiB+TiC
Ti-6Al-4 V	8	2	0	0	Balance	0
5% (TiB+TiC)/Ti-6Al-4V	7.75	1.89	0.62	0.4	Balance	5
8% (TiB+TiC)/Ti-6Al-4V	7.45	1.79	0.992	0.64	Balance	8

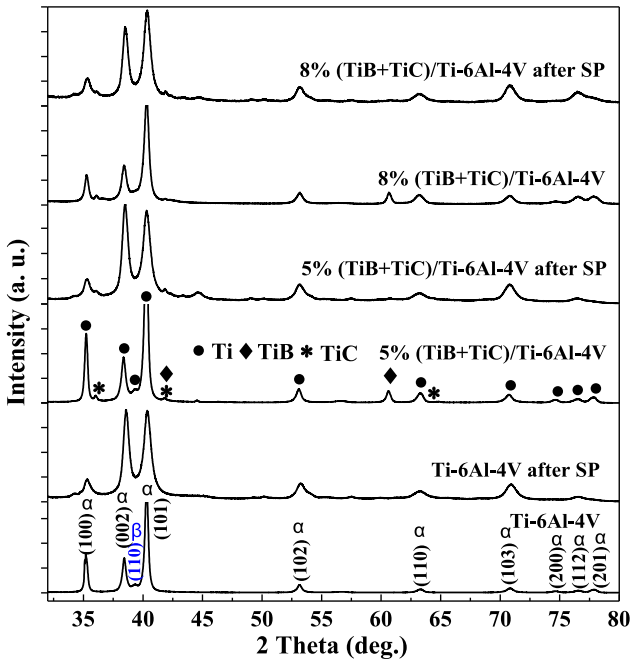

Fig. 2. XRD patterns of Ti-6Al-4V and TMCs before and after SP (SP intensity: 0.15 mmA).

the diffraction peaks of Ti, TiB and TiC can be found obviously, and the locations of Ti diffraction in the matrix of 5% (TiB + TiC)/Ti-6Al-4V and 8% (TiB + TiC)/Ti-6Al-4V are same as those in Ti-6Al-4V. The intensities of some peaks increase because of the influence of SP on the preferred orientation. Before SP, the material shows a preferred orientation of (1 0 1) plane, so the diffraction intensity of (1 0 1) is larger than other peaks. After SP, the preferred orientation is changed and the intensities of other peaks increase, especially the (0 0 2) diffraction peak. The variation trend of three main peaks ((1 0 0), (0 0 2) and (1 0 1)) in TMCs are consistent with those of Ti-6Al-4V, and the width of peaks are increased after SP, which are ascribed to the refined grain size on surface. The detailed characterization and discussion will be conducted as follows.

Under SP, the deformation and strain are introduced on the surface of Ti-6Al-4V, as such, the grains are refined and the dislocation density increases. Fig. 3(a) shows that the nanograins are evenly distributed, and the diffraction rings in the selected area electron diffraction (SAED) of Ti-6Al-4V also verifies the existence of nanograins. Similar results were reported in Ref. [59]. Fig. 3(b) indicates the HRTEM image, and there are the lattice distortion and some amorphous regions around the nanograins, which are caused by the impact of shots on grains, resulting in the plastic deformation under SP. Moreover, the atom arrangement at the grain boundary is distorted. After SP, the amorphous structures are introduced in some regions where the deformation is more severe. Some high resolution TEM images of shot peened Ti-6Al-4V have been shown

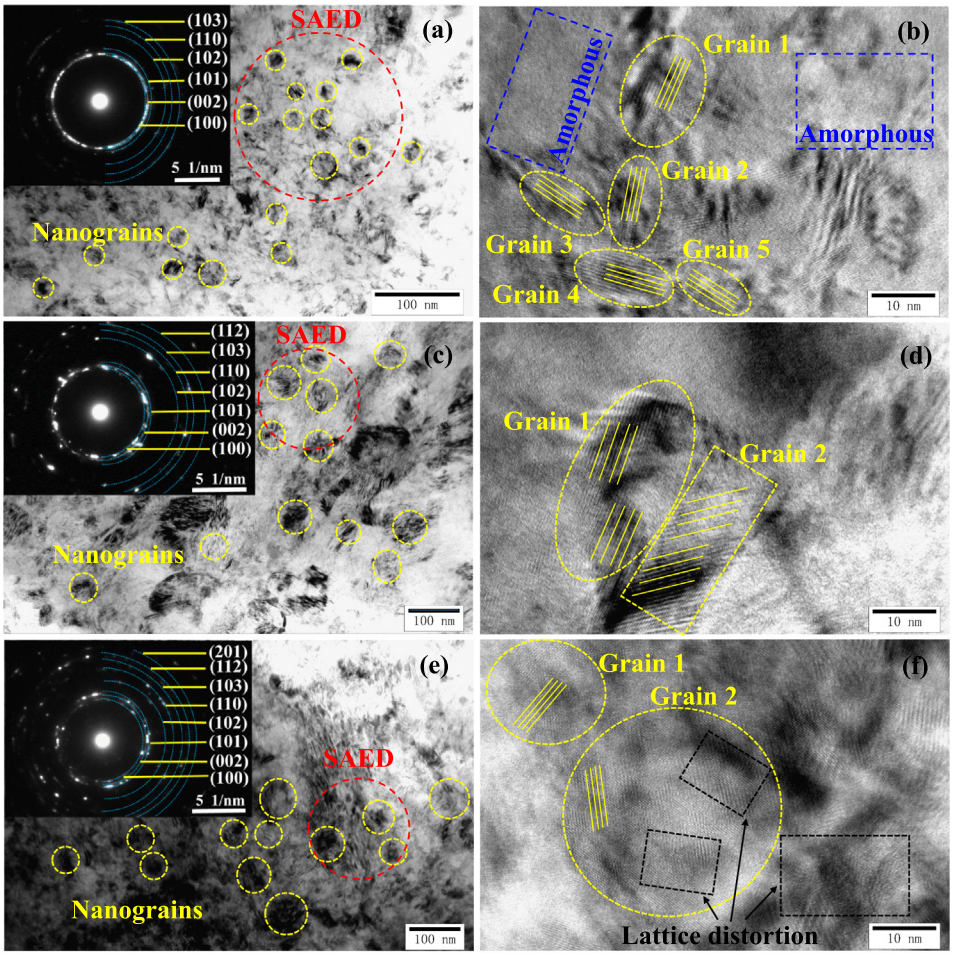

Fig. 3. TEM and HRTEM images of nanograins in the surface of Ti-6Al-4V and (TiB+TiC)/Ti-6Al-4V after SP: (a) the Ti-6Al-4V nanograins; (b) the nanograins in HRTEM and the amorphous region; (c) and (e), the nanograins in the matrix of 5% and 8% (TiB+TiC)/Ti-6Al-4V; (d) and (f), the deformation of nanaograins. The insets in (a), (c) and (e) show the SAED of Ti-6Al-4V.

in Fig. s2 (in Support Information) for the amorphous regions. The disorder atomic arrangement are shown in Fig. s2. From the TEM images, it can be found that the amorphous regions are very small. The atomic arrangements in the amorphous area are disordered, and the deformation is mainly caused by the impact force of shots during SP. Based on Fig. 3(a) and (b), the range of nanograin size is 10–20 nm. The microstructure of matrix in 5% (TiB+TiC)/Ti-6Al-4V after SP is indicated in Fig. 3(c). A large number of nanograins are introduced, and the range of nanograin size is 30–70 nm, which is larger than that in shot peened Ti-6Al-4V. The grains are equivalent to ellipses or circles according to the varition of atom arrangement, and the boundaries of nanograins can be observed based on the magnified TEM images. The area of ellipses can be equivalent to the area of circles. The nanograin size can be determined as the diameter of circles estimately. Fig. 3(d) and (f) show the HRTEM of nanograins in composites. Compared with Ti-6Al-4V, the lattice distortion are found in the nanograins, but the deformation of nanograins are weakened, because the existence of reinforcements can simultaneously hinder the movement of dislocations and reduce the deformation of matrix [60,61]. The microstructures of reinforcements and matrix in 8% (TiB+TiC)/Ti-6Al-4V are shown in Fig. 3(e) and (f). There are many nanograins in the matrix with the size from 20 to 90 nm, which is also larger than that in Ti-6Al-4V, because the existence of reinforcements impede the large deformation of the surface [61]. The nanograin sizes in 8% (TiB + TiC)/Ti-6Al-4V are similar as those in 5% (TiB + TiC)/Ti-6Al-4V. Because of the constant SP intensity and the small difference in the volume fraction of reinforcements, the effect of SP is dominant compared to the influence of reinforcements' volume fraction. The HRTEM image of nanograins in Fig. 3(f) indicates that the lattice distortion is apparent, which is similar as that in 5% (TiB + TiC)/Ti-6Al-4V.

Fig. 4 indicates the microstructure of TiB and the surrounding nanograins in the matrix of 5% (TiB + TiC)/Ti-6Al-4V. A clear interface between TiB and matrix is shown in Fig. 4(a), and the nanograins exist, only a few dislocations are introduced near the edge of TiB. The SAED pattern of TiB is shown in Fig. 4(b). The magnified interfaces shown in Fig. 4(c) and (d) indicate that most area of interfaces are undamaged. A few dislocations are observed, and some smaller nanograins (40–50 nm) are formed near the interface (in Fig. 4(c)) compared to those in Fig. 3(c). However, some dislocations are formed at the corner of TiB during SP (in Fig. 4(e)), which results in the widening of interface to 25–30 nm and the deformation of interface area. The smaller nanograins (40–50 nm) and the dislocations near the interface are caused by the squeeze of matrix to TiB during SP [60,62,63]. The magnified TiB/matrix interface also indicates that severe lattice distortion and dislocations at the interface are formed (in Fig. 4(f)). The matrix near the edge of TiB is deformed more severely under the dual effects of SP and the hindering of TiB, and the refinement of grains is more evident near the interface. The above results indicate that many nanograins are introduced in the matrix, and there is no obvious breakage and cracking in TiB because the SP intensity is 0.15 mmA. Above results reveal that the SP intensity of 0.15 mmA is appropriate for 5% (TiB + TiC)/Ti-6Al-4V.

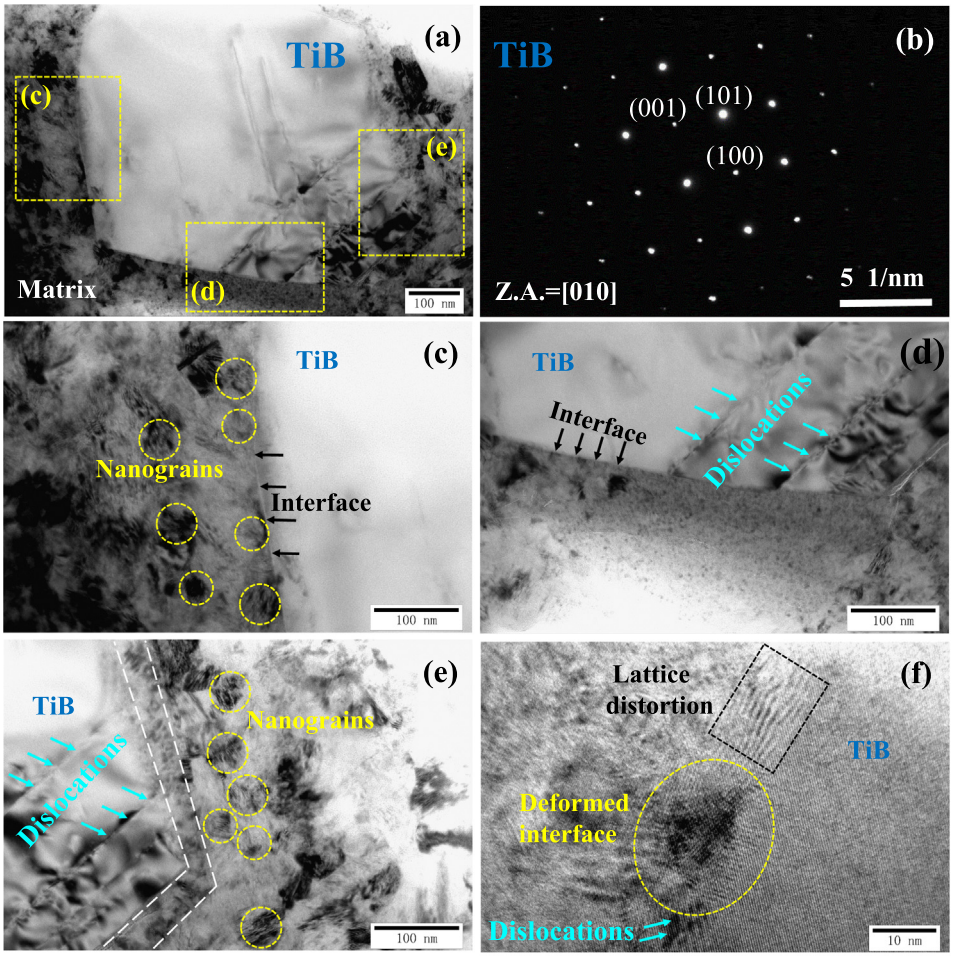

Fig. 4. TEM and HRTEM images of nanograins, TiB and TiB/matrix interface in 5% (TiB+TiC)/Ti-6Al-4V: (a) the morphology of TiB; (b) the SAED pattern; (c) the intact TiB/matrix interface and nanograins around; (d) the interface and dislocations; (e) the widened interface and nanograins around; (f) the HRTEM of deformed interface.

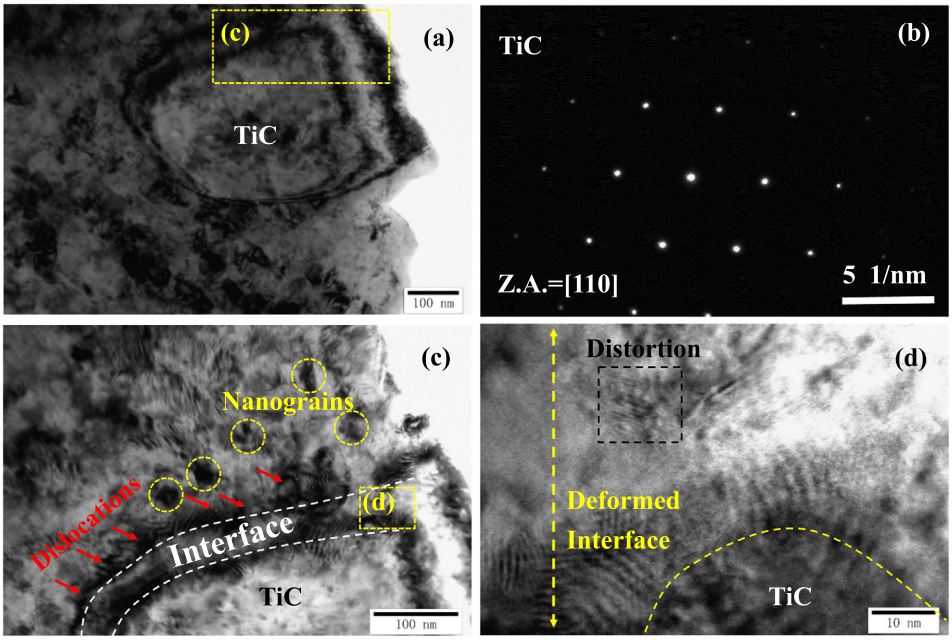

Fig. 5. TEM images of nanograins, TiC and TiC/matrix interface in 5% (TiB+TiC)/Ti-6Al-4V after SP: (a) the morphology of TiC; (b) the SAED pattern; (c) the TiC/matrix interface, nanograins and dislocations near the interface; (d) the magnified interface.

The microstructure of TiC and the nanograins near the interface in 5% (TiB + TiC)/Ti-6Al-4V are indicated in Fig. 5. The morphology of TiC, and a number of nanograins and dislocations are formed around TiC in Fig. 5(a) and (c). The SAED pattern of TiC is shown in Fig. 5(b). Fig. 5(c) indicates the microstructure of TiC/matrix interface, there are more deformation around the interface compared to TiB, which is verified by the widened interface as 40 – 50 nm. The average nanograin size (~ 40 nm) in the matrix around TiC is similar to that around TiB. The HRTEM image of TiC/matrix interface (Fig. 5(d)) shows that the lattice distortion is formed in some areas and some possible morie fringes are generated because of the difference phases between TiC and matrix.

Fig. 6(a)–(c) show the microstructure of TiB/matrix interface and the corners of TiB in 8% (TiB+TiC)/Ti-6Al-4V. As seen from the morphology of TiB corner (Fig. 6(b) and (c)), the clear lattice but no deformation of TiB corner can be observed. The microstructure of TiC, nanograins and TiC/matrix interface are indicated in Fig. 6(d) and (e). Some dislocations and microcracks are formed around TiC, especially at the TiC/matrix interface. The magnified TiC/matrix interface in Fig. 6(e) shows the dislocation walls and

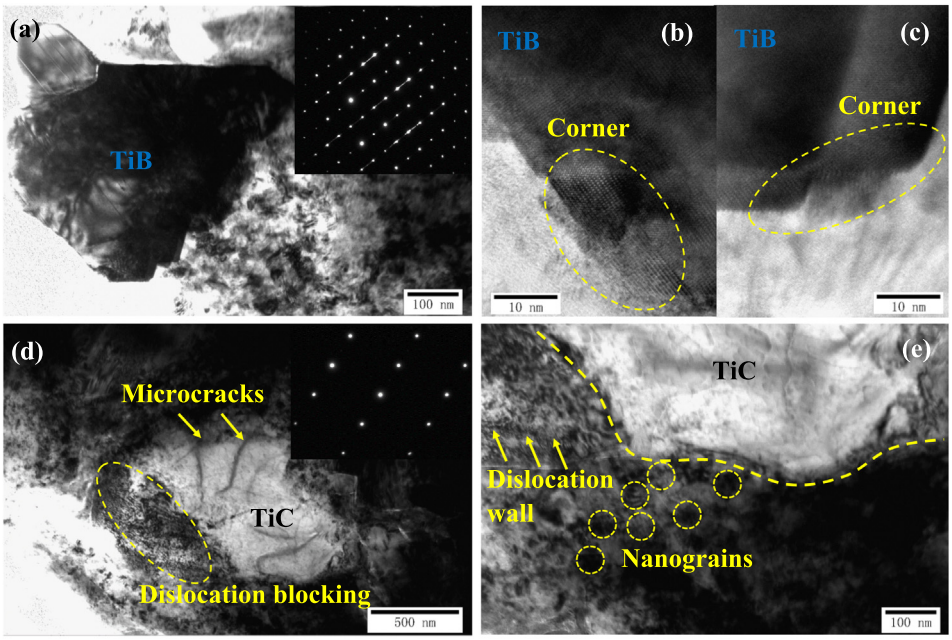

Fig. 6. TEM images of reinforcements and matrix in 8%(TiB+TiC)/Ti-6Al-4V: (a) TiB and nanograins; (b) and (c), HRTEM of TiB/matrix interfaces; (d) TiC, microcracks and dislocations; (e) the dislocations and nanograins near the TiC/matrix interface.

the nanograins near the interface. Compared with TiB, the deformation of TiC is more severe, which is related to the distribution of reinforcements and the impact direction of shots. The impact direction of shots is along the axial direction (Fig. 1) during SP, the shape of TiB is short fibrous but that of TiC is spherical or equiaxed. Therfore, the average impact area between shots and TiC is larger than that of TiB, resulting in the deflection of TiB and the smaller deformation. Moreover, the impact direction of shots is perpendicular to TiC, and the equiaxial TiC could obtain more kinetic energy from the shots. Consequently, more dislocations and defects are blocked at the TiC/matrix interface. Because of the higher volume fraction of reinforcements in 8% (TiB + TiC)/Ti-6Al-4V, the average distance between two reinforcements decreases, which results the matrix near reinforcements be easy to deform under squeezing by both shots and reinforcements. The closer to the reinforcements, the smaller the nanograin size, and the more severe deformation in the matrix.

The microstructures of TiB in 8% (TiB + TiC)/Ti-6Al-4V are displayed in Fig. 7 (a) at low magnification. The intact TiB/matrix interface and the pileup of nanograins near the interface at high magnification are presented in Fig. 7(b). There is no dislocation and defect could be observed in TiB, but the smaller nangrains are introduced near the interface. Besides, the widened TiB/matrix interface (~10 nm) can be observed in Fig. 7(c), which may be caused by that, the matrix at the interface is severely deformed to form amorphous and a few dislocations in the widened interface. Below the widened interface, the intact TiB is free of dislocation and defect, while above the widened interface, there are a large number of smaller nanograins (< 10 nm), which are smaller than that in Fig. 4(c) and (e) in 5% (TiB + TiC)/Ti-6Al-4V and are ascribed to the severe deformation of interface. The potential reason is that the increased volume fraction of reinforcements results in the reduction of the average distance between two reinforcements, which causes the deformation of matrix near reinforcements more severe under squeezing. Moreover, the twinning and faults of TiB are introduced by SP (in Fig. 7(d) and (e)). The HRTEM results indicate that there are continuous twinning and faults near the boundary of TiB, but no apparent dislocations and defects are observed in the middle of TiB (in Fig. 7(d) and (e)). Fig. 7(f) shows the microstructure of TiB/matrix interface. The faults, the deformed interface, the lattice distortion and the nanograins are found near the interface. The squeezing between matrix and interface during SP leads to the interface deformation and lattice distortion.

3.2. Distribution of CRS and hardness

After SP under 0.15 mmA, the distribution of CRS and hardness along the depth are shown in Fig. 8. As shown in Fig. 8(a), the CRS on surface are −374 MPa, −434 MPa and −490 MPa for Ti-6Al-4V, 5% (TiB + TiC)/Ti-6Al-4V, and 8% (TiB + TiC)/Ti-6Al-4V, respectively, and the maximum CRS are −445 MPa, −525 MPa and −595 MPa

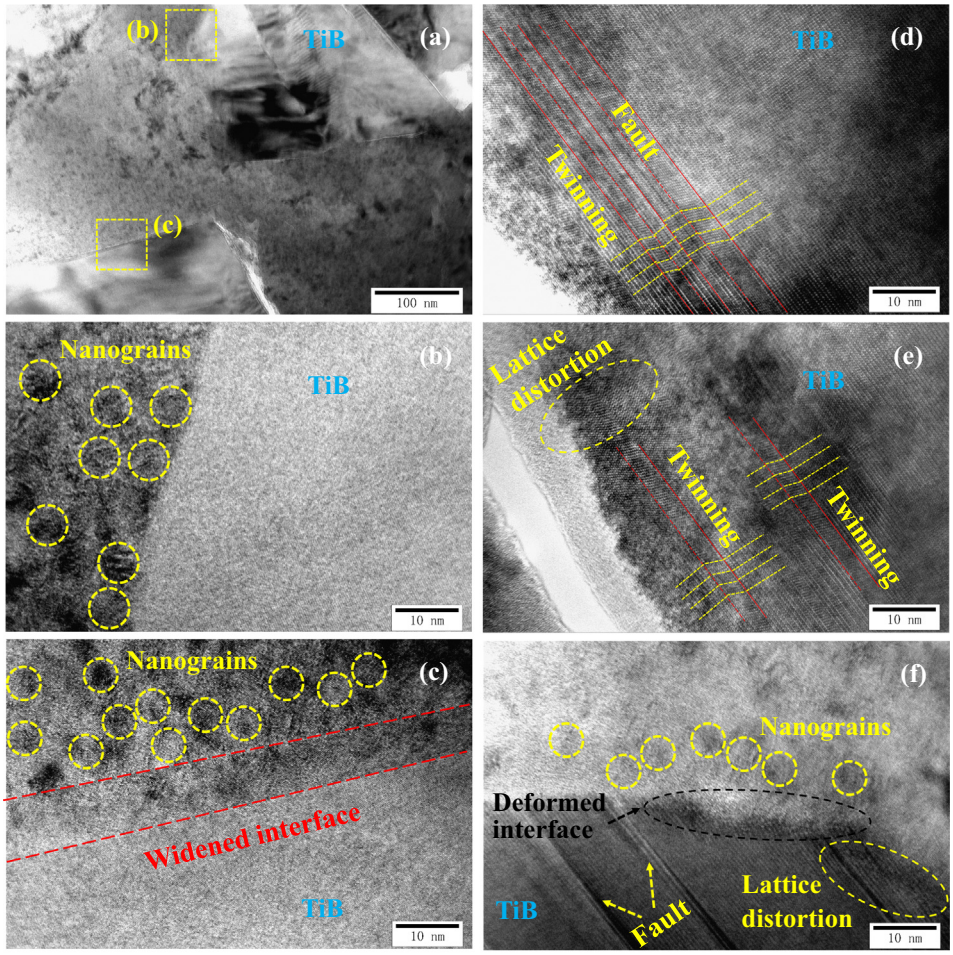

Fig. 7. TEM images of nanograins, TiB, TiB/matrix interface and defects in 8% (TiB+TiC)/Ti-6Al-4V after SP: (a) the morphology of TiB; (b) the intact TiB/matrix interface and the nanograins; (c) the widened TiB/matrix interface and the smaller nanograins around; (d) and (e), the fault and twinning in TiB; (f) the lattice distortion, deformed interface and fault near TiB/matrix interface.

for Ti-6Al-4V, 5% (TiB + TiC)/Ti-6Al-4V, and 8% (TiB + TiC)/Ti-6Al-4V, respectively. The variation of CRS is ascribed to the effect of SP and the distribution of reinforcements at different depths. During SP, the plastic deformation is apt to generate in matrix; however, the existence of reinforcements can restrict the deformation of TMCs, which can promote the CRS in the top surface layer (0–25 μm) and the subsurface layer (25–125 μm). In the deep surface layer (125–300 μm), the dislocation density is lower than that in the top surface layer [50,64], and the blockage effect of reinforcements on the deformation is not apparent, which results in the higher CRS in Ti-6Al-4 V than that in TMCs. After SP, the deformation of near surface layer is more severe than the deep surface layer, so the reinforcements' resistance to the near surface layers' deformation is feeble and the high CRS are introduced finally. However, at the deep surface layer, the effect of reinforcements' resistance shows obviously. Consequently, the decrease rates of CRS in TMC are faster than the matrix's. As seen from Fig. 8(b), the hardness displays significant increment in the surface layer after SP. The surface average hardness reaches 474 HV, 512 HV and 575 HV for Ti-6Al-4V, 5% (TiB + TiC)/Ti-6Al-4V, 8% (TiB + TiC)/Ti-6Al-4V respectively, which are exceeding 50% higher than the hardness of Ti-6Al-4V before SP (~ 310 HV). The CRS are introduced by the deformation of matrix and reinforcements after SP, and the increase in hardness is owing to the formation of nanograins and the high dislocation density.

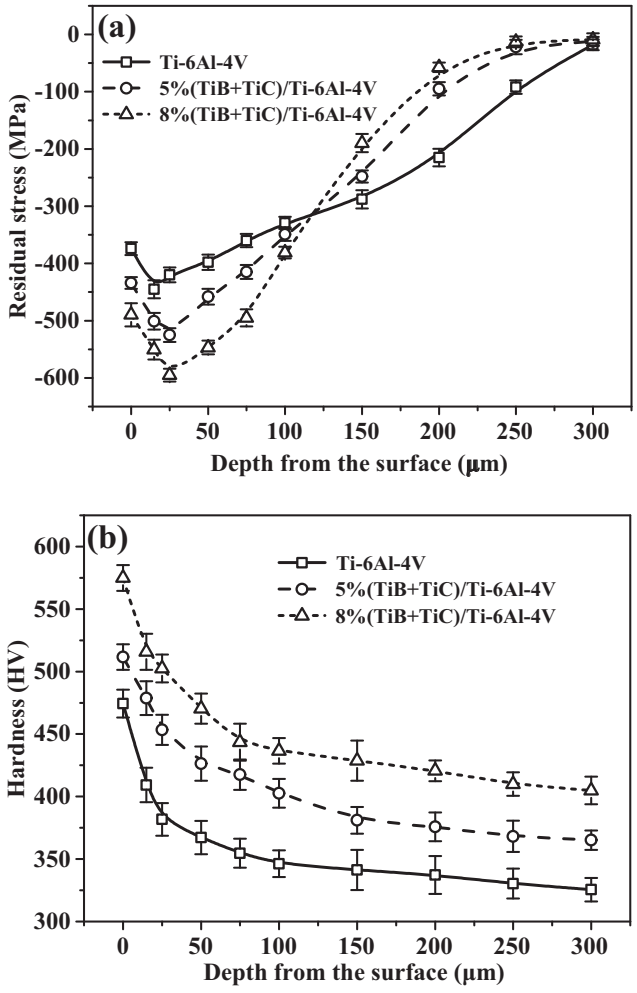

Fig. 8. The distribution of CRS and hardness along the depth from the top surface under the SP intensity of 0.15 mmA: (a) CRS; (b) hardness.

4. Discussion

Based on above characterization and analysis, the schematics of microstructure variation before and after SP are shown in Fig. 9, including the deformation of reinforcements and matrix, and the nanocrystal layer. As shown in Fig. 9(a), the nanocrystal layer is formed on the surface of Ti-6Al-4V after SP, and the size of nanograins increases gradually from the top surface (10–20 nm) to the subsurface (> 100 nm), because the top surface is substantially influenced by SP while the deep layer is less affected by SP and with less deformation [65,66]. The closer to the top surface, more severe the deformation of surface layer. Furthermore, the local amorphous region near the top surface is formed due to the severe deformation on the top surface under SP. Fig. 9(b) shows the nanograin distribution and the deformation of reinforcements after SP in 5% (TiB + TiC)/Ti-6Al-4V. Under the same SP intensity, the nanocrystal and deformation layer is also formed in the surface layer; however, the thickness of deformation layer (~ 250 nm) is smaller than that in the peened Ti-6Al-4V (~ 300 nm), and the size of nanograins (30–70 nm) is larger than that in the peened Ti-6Al-4V. Besides, the reinforcements in the surface layer are deformed and the deformation of TiC is more severe than that of TiB, as indicated by the dotted line in Fig. 9(b), which is due to the different shapes and distribution of reinforcements, as well as the impact direction of shots during SP. Fig. 9(c) shows the schematic of nanograins and the deformation of reinforcements after SP in 8% (TiB + TiC)/Ti-6Al-4V. The nanograins are also introduced and the size (20–90 nm) is close to that of peened 5% (TiB + TiC)/Ti-6Al-4V. However, the deformation of reinforcements become more severe, and the smaller nanograins (<10 nm) are formed near the reinforcement/matrix interface (in Fig. 9(c)), because the distance between two reinforcements is reduced with the increase in volume fraction of reinforcements, thereby resulting in severe deformation between matrix and reinforcements. As such, the smaller nanograins are introduced near the interface. Based on the references [67,68], the gradient structure with the refined grains and the dislocation density could improve the mechanical properties

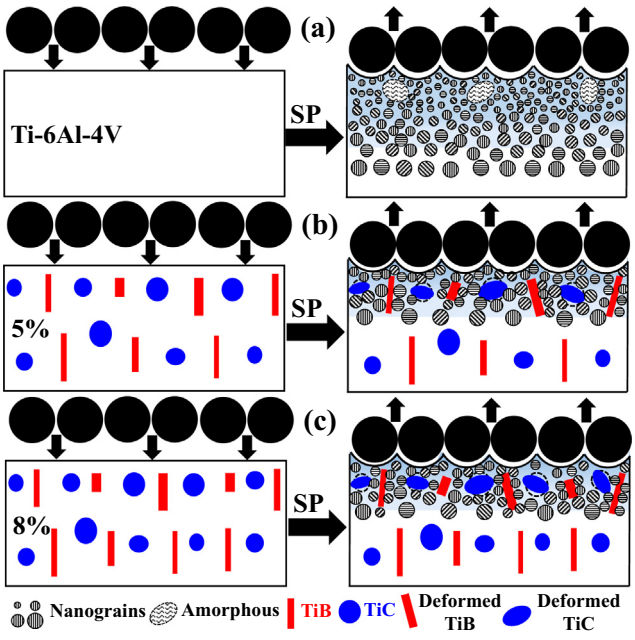

Fig. 9. Schematics of microstructure variation before and after SP: (a) the formation of nanograins in Ti-6Al-4V; (b) the deformation of reinforcements and matrix in 5% (TiB+TiC)/Ti-6Al-4V; (c) the deformation of reinforcements and matrix in 8% (TiB +TiC)/Ti-6Al-4V.

of metals, which can be concluded from the results of CRS and hardness. Summary, under the SP intensity of 0.15 mmA, the nanocrystal and deformation layer were formed in the surface layer, resulting in the improvement of CRS and surface hardness, which could be beneficial for modifing the mechanical performances of shot peened TMCs.

5. Conclusions

The surface microstructure and mechanical properties of shot peened layer in (TiB+TiC)/Ti-6Al-4V were characterized and analyzed in detail. Some important results have been obtained.

(1) After SP, the nanocrystal and deformation layers were introduced on Ti-6Al-4V and (TiB+TiC)/Ti-6Al-4V, and the size of nanograins were influenced by the shapes, distribution and volume fraction of reinforcements.
(2) The increase in the volume fraction of reinforcements reduced the average distance between two reinforcements, causing the more severe deformation of the matrix and the formation of smaller nanograins near the interface, because the matrix was squeezed by both the shots and the reinforcements during SP.
(3) The existence of reinforcements could hinder the deformation of TMCs. The deformation of TiC was more severe than that of TiB, and more dislocations were introduced in the matrix around TiC, which were ascribed to the different shapes and distribution of TiB and TiC, and the impact direction of shots during SP.
(4) The high CRS were introduced in the peened surface, and the maximum CRS was −595 MPa. The surface hardness of specimen was enhanced and the maximum value was 575 HV. The nanocrystal and deformation layer were formed in the surface layer, resulting in the improvement of CRS and surface hardness, which could be beneficial for modifing the mechanical performances of shot peened TMCs.

6. Data availability

The raw/processed data required to reproduce these findings cannot be shared at this time as the data also forms part of an ongoing study.

CRediT authorship contribution statement

Yan Wen: Investigation, Methodology, Writing - original draft. **Yaya Wu:** Investigation, Validation, Writing - original draft. **Lin Hua:** Supervision, Writing - review & editing. **Lechun Xie:** Supervision, Writing - review & editing. **Liqiang Wang:** Writing - review & editing. **Lai-Chang Zhang:** Writing - review & editing. **Weijie Lu:** Writing - review & editing.

Declaration of Competing Interest

The authors declare that they have no known competing financial interests or personal relationships that could have appeared to influence the work reported in this paper.

Acknowledgements

This work was financial supported by National Key R&D Program of China (No. 2020YFA0714900), National Natural Science Foundation of China (Grant No. 51901165, No. 51975441), Application Foundation Frontier Project of Wuhan (No. 2020010601012171), "Chu Tian Scholar" project of Hubei Province (CTXZ2017-05), Overseas Expertise Introduction Project for Discipline Innovation (B17034) and Innovative Research Team Development Program of Ministry of Education of China (IRT_17R83).

Appendix A. Supplementary material

Supplementary data to this article can be found online at https://doi.org/10.1016/j.matdes.2021.109760.

References

[1] S.C. Tjong, Z. Ma, Microstructural and mechanical characteristics of in situ metal matrix composites, Mater. Sci. Eng., R 29 (2000) 49–113.
[2] L.-C. Zhang, J. Xu, J. Eckert, Thermal stability and crystallization kinetics of mechanically alloyed TiC/Ti-based metallic glass matrix composite, J. Appl. Phys. 100 (2006) 033514.
[3] L.-C. Zhang, H. Attar, Selective Laser Melting of Titanium Alloys and Titanium Matrix Composites for Biomedical Applications: A Review Adv, Eng. Mater. 18 (2016) 463–475.
[4] L.-C. Zhang, L.-Y. Chen, A Review on Biomedical Titanium Alloys: Recent Progress and Prospect, Adv. Eng. Mater. 21 (2019) 1801215.
[5] L. Xie, L. Wang, K. Wang, G. Yin, Y. Fu, D. Zhang, W. Lu, L. Hua, L.-C. Zhang, TEM characterization on microstructure of Ti–6Al–4V/Ag nanocomposite formed by friction stir processing, Materialia 3 (2018) 139–144.
[6] L. Wang, L. Xie, P. Shen, Q. Fan, W. Wang, K. Wang, W. Lu, L. Hua, L.-C. Zhang, Surface microstructure and mechanical properties of Ti-6Al-4V/Ag nanocomposite prepared by FSP, Mater. Charact. 153 (2019) 175–183.
[7] L. Huang, L. Geng, Discontinuously Reinforced Titanium Matrix Composites, Springer, 2017.
[8] L. Huang, L. Geng, H. Peng, Microstructurally inhomogeneous composites: is a homogeneous reinforcement distribution optimal?, Prog. Mater Sci. 71 (2015) 93–168.
[9] L.C. Zhang, Y. Liu, S. Li, Y. Hao, Additive manufacturing of titanium alloys by electron beam melting: A review, Adv. Eng. Mater. 20 (2018) 1700842.
[10] G. Lütjering, J.C. Williams, Titanium Matrix Composites, in: Springer Titanium (Ed.), Berlin Heidelberg, Heidelberg, Berlin, 2007, pp. 367–382.
[11] A. Mortensen, J. Llorca, Metal matrix composites, Annu. Rev. Mater. Res. 40 (2010) 243–270.
[12] G.H. Feng, Y.Q. Yang, X. Luo, J. Li, B. Huang, Y. Chen, Fatigue properties and fracture analysis of a SiC fiber-reinforced titanium matrix composite, Composites Part B 68 (2015) 336–342.
[13] L. Wagner, Mechanical surface treatments on titanium, aluminum and magnesium alloys, Mater. Sci. Eng., A 263 (1999) 210–216.
[14] H. Lee, S. Mall, Stress relaxation behavior of shot-peened Ti–6Al–4V under fretting fatigue at elevated temperature, Mater. Sci. Eng., A 366 (2004) 412–420.
[15] P.J. Golden, A. Hutson, V. Sundaram, J.H. Arps, Effect of surface treatments on fretting fatigue of Ti–6Al–4V, Int. J. Fatigue 29 (2007) 1302–1310.
[16] Y. Geng, X. Mei, K. Wang, X. Dong, X. Yan, Z. Fan, W. Duan, W. Wang, Effect of Laser Shock Peening on Residual Stress, Microstructure and Hot Corrosion Behavior of Damage-Tolerant TC21 Titanium Alloy, J. Mater. Eng. Perform. 27 (2018) 4703–4713.
[17] L. Wang, L. Xie, Y. Lv, L.-C. Zhang, L. Chen, Q. Meng, J. Qu, D. Zhang, W. Lu, Microstructure evolution and superelastic behavior in Ti-35Nb-2Ta-3Zr alloy processed by friction stir processing, Acta Mater. 131 (2017) 499–510.
[18] C. Zhang, Z. Ding, L. Xie, L.-C. Zhang, L. Wu, Y. Fu, L. Wang, W. Lu, Electrochemical and in vitro behavior of the nanosized composites of Ti-6Al-4V and TiO2 fabricated by friction stir process, Appl. Surf. Sci. 423 (2017) 331–339.
[19] G. Louarn, L. Salou, A. Hoornaert, P. Layrolle, Nanostructured surface coatings for titanium alloy implants, J. Mater. Res. 1–8 (2019).
[20] S. Tekeli, Enhancement of fatigue strength of SAE 9245 steel by shot peening, Mater. Lett. 57 (2002) 604–608.
[21] V. Fridrici, S. Fouvry, P. Kapsa, Effect of shot peening on the fretting wear of Ti–6Al–4V, Wear 250 (2001) 642–649.
[22] G. Webster, A. Ezeilo, Residual stress distributions and their influence on fatigue lifetimes, Int. J. Fatigue 23 (2001) 375–383.
[23] J.D. Almer, J. Cohen, R. Winholtz, The effects of residual macrostresses and microstresses on fatigue crack propagation, Metall. Mater. Trans. A 29 (1998) 2127–2136.
[24] J. Almer, J. Cohen, B. Moran, The effects of residual macrostresses and microstresses on fatigue crack initiation, Mater. Sci. Eng., A 284 (2000) 268–279.
[25] P. Zhang, J. Lindemann, Influence of shot peening on high cycle fatigue properties of the high-strength wrought magnesium alloy AZ80, Scr. Mater. 52 (2005) 485–490.
[26] G. Farrahi, J. Lebrijn, D. Couratin, Effect of shot peening on residual stress and fatigue life of a spring steel, Fatigue Fract. Eng. Mater. Struct. 18 (1995) 211–220.
[27] V. Schulze, Characteristics of surface layers produced by shot peening, in: Proceeding of the Eighth International Conference on Shot Peening ICSP-8 in Garmisch-Partenkirchen DGM, Citeseer, 2002, 145–160.

[28] L. Xie, Y. Wen, K. Zhan, L. Wang, C. Jiang, V. Ji, Characterization on surface mechanical properties of Ti–6Al–4V after shot peening, J. Alloys Compd. 666 (2016) 65–70.
[29] H. Ishigami, K. Matsui, Y. Jin, K. Ando, Technical note A study on stress, reflection and double shot peening to inrease compressive residual stress, Fatigue Fract. Eng. Mater. Struct. 23 (2000) 959–963.
[30] W. Luan, C. Jiang, V. Ji, Surface layer characteristics of TiB2/Al composite by stress peening, Mater. Trans. 50 (2009) 837–840.
[31] L. Xie, C. Jiang, W. Lu, Y. Chen, J. Huang, Effect of stress peening on surface layer characteristics of (TiB + TiC)/Ti–6Al–4V composite, Mater. Des. 33 (2012) 64–68.
[32] L. Xie, C. Jiang, W. Lu, K. Zhan, Y. Chen, Investigation on the residual stress and microstructure of (TiB + TiC)/Ti–6Al–4V composite after shot peening, Mater. Sci. Eng., A 528 (2011) 3423–3427.
[33] Z. Zhang, M. Lin, D.H.L. Seng, S.L. Teo, F. Wei, H.R. Tan, A.K.H. Cheong, S.H. Lim, S. Wang, J. Pan, Fatigue life enhancement in alpha/beta Ti–6Al–4V after shot peening: An EBSD and TEM crystallographic orientation mapping study of surface layer, Materialia 12 (2020) 100813.
[34] C. Zhang, T. Fu, H. Chen, Y. Gao, Microstructure Evolution of Surface Gradient Nanocrystalline by Shot Peening of TA17 Titanium Alloy, Metall. Mater. Trans. A (2021).
[35] S. Kumar, K. Chattopadhyay, G. Mahobia, V. Singh, Hot corrosion behaviour of Ti–6Al–4V modified by ultrasonic shot peening, Mater. Des. 110 (2016) 196–206.
[36] S. Slawik, S. Bernarding, F. Lasagni, C. Navarro, A. Periñán, F. Boby, S. Migot-Choux, J. Domínguez, F. Mücklich, Microstructural analysis of selective laser melted Ti6Al4V modified by laser peening and shot peening for enhanced fatigue characteristics, Mater. Charact. 173 (2021) 110935.
[37] M. Logesh, R. Selvabharathi, T. Thangeeswari, S. Palani, Influence of severe double shot peening on microstructure properties of Ti 6Al-4V and Titanium Grade 2 dissimilar joints using laser beam welding, Opt. Laser Technol. 123 (2020) 105883.
[38] J. Chi, Z. Cai, H. Zhang, H. Zhang, W. Guo, Z. Wan, G. Han, P. Peng, Z. Zeng, Combining manufacturing of titanium alloy through direct energy deposition and laser shock peening processes, Mater. Des. 203 (2021) 109626.
[39] X. Ma, Z. Chen, D. Zhong, S.N. Luo, L. Xiao, W. Lu, S. Zhang, Effect of rotationally accelerated shot peening on the microstructure and mechanical behavior of a metastable β titanium alloy, J. Mater. Sci. Technol. 75 (2021) 27–38.
[40] Y. Wang, Y. Zhang, G. Song, W. Niu, Z. Xu, C. Huang, Effect of shot peening on fatigue crack propagation of Ti6Al4V, Mater. Today Commun. 25 (2020) 101430.
[41] X.-T. Luo, Y.-K. Wei, Y. Wang, C.-J. Li, Microstructure and mechanical property of Ti and Ti6Al4V prepared by an in-situ shot peening assisted cold spraying, Mater. Des. 85 (2015) 527–533.
[42] Q. Zhang, B. Duan, Z. Zhang, J. Wang, C. Si, Effect of ultrasonic shot peening on microstructure evolution and corrosion resistance of selective laser melted Ti–6Al–4V alloy, J. Mater. Res. Technol. 11 (2021) 1090–1099.
[43] C. Yang, Y.G. Liu, Y.H. Shi, M.Q. Li, Microstructure characterization and tensile properties of processed TC17 via high energy shot peening, Mater. Sci. Eng., A 784 (2020) 139298.
[44] L. Tan, C. Yao, D. Zhang, J. Ren, Z. Zhou, J. Zhang, Evolution of surface integrity and fatigue properties after milling, polishing, and shot peening of TC17 alloy blades, Int. J. Fatigue 136 (2020) 105630.
[45] S. Bagherifard, I. Fernandez-Pariente, R. Ghelichi, M. Guagliano, Fatigue behavior of notched steel specimens with nanocrystallized surface obtained by severe shot peening, Mater. Des. 45 (2013) 497–503.
[46] S. Bagherifard, S. Slawik, I. Fernández-Pariente, C. Pauly, F. Mücklich, M. Guagliano, Nanoscale surface modification of AISI 316L stainless steel by severe shot peening, Mater. Des. 102 (2016) 68–77.
[47] N. Sidhom, A. Laamouri, R. Fathallah, C. Braham, H.P. Lieurade, Fatigue strength improvement of 5083 H11 Al-alloy T-welded joints by shot peening: experimental characterization and predictive approach, Int. J. Fatigue 27 (2005) 729–745.
[48] Y.F. Al-Obaid, The effect of shot peening on stress corrosion cracking behaviour of 2205-duplex stainless steel, Eng. Fract. Mech. 51 (1995) 19–25.
[49] L. Xie, C. Wang, L. Wang, Z. Wang, C. Jiang, W. Lu, V. Ji, Numerical analysis and experimental validation on residual stress distribution of titanium matrix composite after shot peening treatment, Mech. Mater. 99 (2016) 2–8.
[50] L. Xie, C. Jiang, W. Lu, Q. Feng, X. Wu, Investigation on the surface layer characteristics of shot peened titanium matrix composite utilizing X-ray diffraction, Surf. Coat. Technol. 206 (2011) 511–516.
[51] L. Xie, C. Jiang, W. Lu, K. Zhan, Q. Feng, X. Wu, F. Wang, The recrystallization behavior of surface deformation layer of (TiB+TiC)/Ti–6Al–4V composite during isothermal annealing, Mater. Sci. Eng., A 530 (2011) 239–243.
[52] L. Xie, C. Jiang, W. Lu, The influence of shot peening on the surface properties of (TiB+ TiC)/Ti–6Al–4V, Appl. Surf. Sci. 280 (2013) 981–988.
[53] L. Xie, Q. Feng, Y. Wen, L. Wang, C. Jiang, W. Lu, Surface microstructure characterization on shot peened (TiB+ TiC)/Ti–6Al–4V by Rietveld whole pattern fitting method, J. Mater. Res. 31 (2016) 2291–2301.
[54] W. Lu, D. Zhang, X. Zhang, R. Wu, T. Sakata, H. Mori, Microstructural characterization of TiB in in situ synthesized titanium matrix composites prepared by common casting technique, J. Alloys Compd. 327 (2001) 240–247.
[55] L. Xie, Q. Zhou, X. Jin, Z. Wang, C. Jiang, W. Lu, J. Wang, Q. Jane Wang, Effect of reinforcements on rolling contact fatigue behaviors of titanium matrix composite (TiB + TiC)/Ti–6Al–4V, Int. J. Fatigue 66 (2014) 127–137.
[56] W. Lu, D. Zhang, X. Zhang, R. Wu, T. Sakata, H. Mori, HREM study of TiB/Ti interfaces in a TiB-TiC in situ composite, Scr. Mater. 44 (2001) 1069–1075.
[57] L. Xie, L. Wang, C. Jiang, W. Lu, The variations of microstructures and hardness of titanium matrix composite (TiB+ TiC)/Ti–6Al–4V after shot peening, Surf. Coat. Technol. 244 (2014) 69–77.
[58] P. Withers, H. Bhadeshia, Residual stress. Part 1–measurement techniques, Mater. Sci. Technol. 17 (2001) 355–365.
[59] Y.G. Liu, M.Q. Li, H.J. Liu, Nanostructure and surface roughness in the processed surface layer of Ti-6Al-4V via shot peening, Mater. Charact. 123 (2017) 83–90.
[60] X. Guo, L. Wang, M. Wang, J. Qin, D. Zhang, W. Lu, Effects of degree of deformation on the microstructure, mechanical properties and texture of hybrid-reinforced titanium matrix composites, Acta Mater. 60 (2012) 2656–2667.
[61] L. Huang, Q. An, L. Geng, S. Wang, S. Jiang, X. Cui, R. Zhang, F. Sun, Y. Jiao, X. Chen, C. Wang, Multiscale Architecture and Superior High-Temperature Performance of Discontinuously Reinforced Titanium Matrix Composites, Adv. Mater. 33 (2021) 2000688.
[62] S. Sun, W. Lu, Effects of trace reinforcements on microstructure and tensile properties of in-situ synthesized TC18 Ti matrix composite, J. Compos. Mater. 51 (2017) 3623–3629.
[63] S. Sun, M. Wang, L. Wang, J. Qin, W. Lu, D. Zhang, The influences of trace TiB and TiC on microstructure refinement and mechanical properties of in situ synthesized Ti matrix composite, Composites Part B 43 (2012) 3334–3337.
[64] K. Zhan, Y. Wu, J. Li, B. Zhao, Y. Yan, L. Xie, L. Wang, V. Ji, Investigation on surface layer characteristics of shot peened graphene reinforced Al composite by X-ray diffraction method, Appl. Surf. Sci. 435 (2018) 1257–1264.
[65] A.A. Ahmed, M. Mhaede, M. Wollmann, L. Wagner, Effect of micro shot peening on the mechanical properties and corrosion behavior of two microstructure Ti–6Al–4V alloy, Appl. Surf. Sci. 363 (2016) 50–58.
[66] J.Z. Lu, L.J. Wu, G.F. Sun, K.Y. Luo, Y. Zhang, J. Cai, C.Y. Cui, X.M. Luo, Microstructural response and grain refinement mechanism of commercially pure titanium subjected to multiple laser shock peening impacts, Acta Mater. 127 (2017) 252–266.
[67] K. Lu, Making strong nanomaterials ductile with gradients, Science 345 (2014) 1455–1456.
[68] T.H. Fang, W. Li, N.R. Tao, K. Lu, Revealing Extraordinary Intrinsic Tensile Plasticity in Gradient Nano-Grained Copper, Science 331 (2011) 1587–1590.